Geophysical Journal International

Geophys. J. Int. (2013) **193,** 161–170 doi: 10.1093/gji/ggs135

Monitoring Santorini volcano (Greece) breathing from space

Michael Foumelis,[1] Elisa Trasatti,[2] Elena Papageorgiou,[3] Salvatore Stramondo[2] and Issaak Parcharidis[4]

[1]*Science, Applications and Future Technology Department, European Space Agency (ESA-ESRIN), Via Galileo Galilei,* 00044 *Frascati, Italy. E-mail: michael.foumelis@esa.int*

[2]*Centro Nazionale Terremoti, Istituto Nazionale di Geofisica e Vulcanologia (INGV),* 605*, Via di Vigna Murata,* 00143 *Rome, Italy*

[3]*Institute of Acoustics and Sensors, National Research Council of Italy (CNR),* 100*, Via del Fosso del Cavaliere,* 00133 *Rome, Italy*

[4]*Department of Geography, Harokopio University of Athens,* 70*, El. Venizelou Str.,* 17671 *Kallithea, Athens, Greece*

Accepted 2012 December 31. Received 2012 December 21; in original form 2012 October 17

SUMMARY

Since its last eruption in 1950, Santorini volcano (Greece) remained in a dormant state. This is also evidenced for the period 1992–2010 by the gradual deflation signal over Nea Kameni as measured by satellite Synthetic Aperture Radar Interferometry (InSAR) with low rates of about 5–6 mm yr^{-1} as well as by the absence of seismic activity within the caldera. However, at the beginning of 2011 the volcano showed signs of unrest with increased microseismic activity and significant ground uplift, reaching 14 cm within a year (2011 March–2012 March), according to InSAR time-series. ALOS PALSAR data indicate the onset of the phenomenon in early 2010 where an aseismic pre-unrest phase of increased subsidence (1–3 cm) preceded the uplift. Joint inversions of SAR and GPS velocities using spherical and spheroidal magmatic source types indicate their location offshore at about 1 km north of Nea Kameni and between 3.5 and 3.8 km depth. The estimated volume variation rate is 6×10^6 m^3 yr^{-1} to 9×10^6 m^3 yr^{-1}. A gradual slowing in the rate of inflation within the first quarter of 2012 is apparent by ENVISAT data, while subsequent observations from RADARSAT-2 confirm the observed trend.

Key words: Radar interferometry; Remote sensing of volcanoes; Volcano monitoring.

1 INTRODUCTION

Santorini comprises the most active volcanic centre in the Aegean Sea (Greece), and is documented to have given one of the largest volcanic events known in historical time (Friedrich *et al.* 2006; Druitt *et al.* 2012); the so-called Minoan eruption, which occurred in the late 1600s BC with major catastrophic effects (McCoy & Dunn 2002; Sigurdsson *et al.* 2006), entailed the establishment of a flooded caldera up to almost 400 m depth, while the caldera walls rising 300–400 m above sea level form a characteristic ring of islands (Fig. 1). Post-Minoan volcanic activity of multiple caldera collapses and magma depositions, was almost entirely confined within the caldera, in the central part of which Palea and Nea Kameni volcanic centres emerged (Fytikas *et al.* 1990; Druitt *et al.* 1999; Vougioukalakis & Fytikas 2005). Exception is considered the eruption of 1650 AD associated with the submarine Columbos volcano 6.5 km offshore of Thera (Fouqué 1879; Chiodini *et al.* 1996; Dominey-Howes *et al.* 2000; Nomikou *et al.* 2012).

The last eruptive cycle of Santorini of four periods of explosive volcanic activity from 1925 to 1950 in Nea Kameni (Georgalas 1962), was resumed by a repose period of fumarolic activity and thermal venting (Chiodini *et al.* 1998). Seismological indications describe the presence of two active magma chambers below Nea Kameni and Columbos volcanoes (Delibasis *et al.* 1989). The local seismicity shows high seismic activity in the surroundings of Columbos volcano area and fairly low activity at the rest of the complex (Bohnhoff *et al.* 2006; Dimitriadis *et al.* 2009) (Fig. 1). However, at the beginning of 2011 the volcano showed signs of unrest with an increase in the rate of microseismicity within the intracaldera area (http://bbnet.gein.noa.gr). The unrest episode was expressed in addition with substantial amounts of ground uplift, denoting the justification of the volcanic origin of the activity (Papageorgiou *et al.* 2012). Still, the induced quasi-radial deformation was imaged by a dense network of continuous and campaign GPS stations and a volumetric expansion of 14×10^6 m^3 of a spherical source located in the northern caldera at 4 km depth, was finally identified (Newman *et al.* 2012). A similar shallow source with a volume variation of 10×10^6 m^3 to 20×10^6 m^3 and depth 4.4 km is suggested by Parks *et al.* (2012), using Synthetic Aperture Radar Interferometry (InSAR) data.

Magma emplacement at depth is considered to be the dominant source of caldera unrest (Dzurisin 2003). Thus, during a paroxysmal period, magma motion assumes the primary role and deformation may serve as a precursor to eruptive activity. SAR Interferometry is widely used in ground deformation monitoring with explicit efficacy on applications where volcanic induced deformation is being studied (Massonnet *et al.* 1995; Rosen *et al.* 1996; Sigmundsson *et al.* 1999; Pritchard & Simons 2002; Hooper *et al.* 2004; Tizzani *et al.* 2007).

In this paper advanced InSAR techniques were applied in Santorini to reveal the deformation field before (1992–2010) and during (2011–2012) the inflationary episode. A comprehensive analysis of

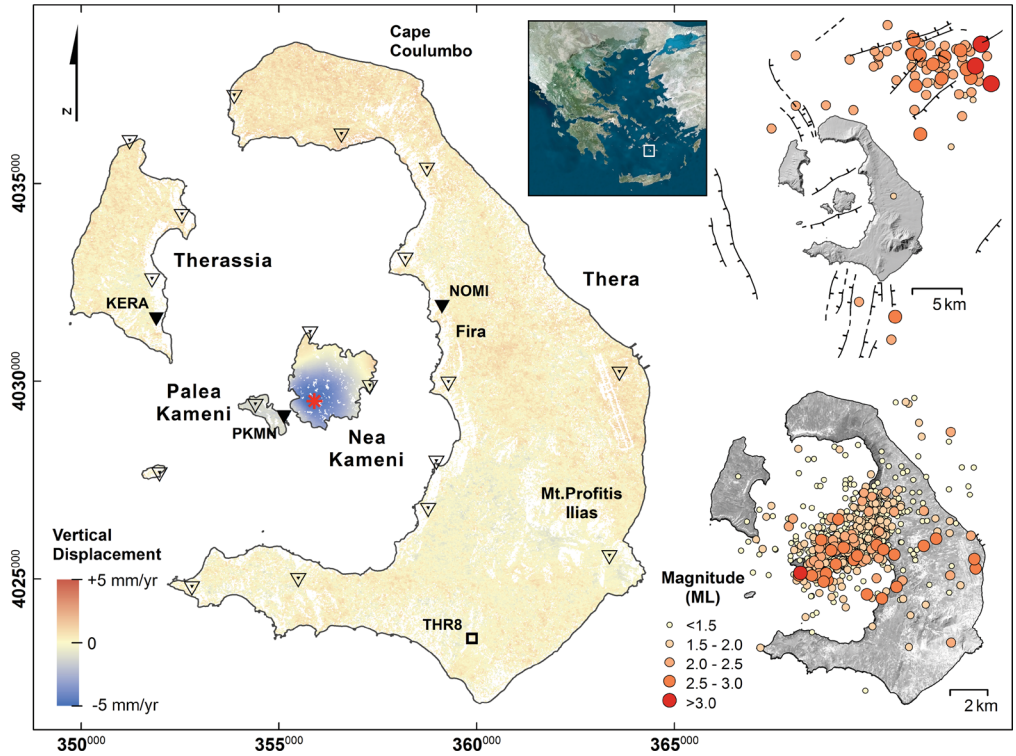

Figure 1. Vertical ground surface displacement rates for the period of 1992–2010 (18 yr), calculated based on ERS-ENVISAT ascending and descending data. Local reference point (THR8, after Newman *et al.* 2012) is denoted as square. The star marks the inferred location of the Mogi source (see text). Triangles indicate geodetic GPS stations from Newman *et al.* (2012), continuous (black) and campaign sites (transparent). The regional seismicity of the area between 2000 and 2010 (rest phase; AUTH) and the main fault systems (Perissoratis 1995) are shown (upper right corner), whereas the contemporary seismic activity during the unrest episode (AUTH, 2011 January–2011 June and NOA, 2011 July–2012 March) is also given (lower right corner).

multisensor SAR acquisitions from ERS, ENVISAT, ALOS and RADARSAT-2 satellite missions, is performed to monitor the long-term deformation history of the volcanic complex, whereas the observed ground displacements are investigated in terms of modelled volcanic sources by joint inversion of SAR and GPS geodetic data. The temporal evolution of deformation deduced by InSAR data provided detailed insights on the deformation pattern immediately before the inflation, the onset of the phenomenon as well as the state of the volcano during the closure of this volcanic episode.

2 SAR DATA AND INTERFEROMETRIC PROCESSING

The entire archives of ERS-1/-2 SAR and ENVISAT ASAR C-band data (IS2), comprising 30 and 66 scenes in ascending (track 329) and descending (track 150) orbits, respectively, were utilized to investigate the displacement field of Santorini during its dormant phase covering a time span of about 18 yr (1992 June–2010 May). Additional L-band data from ALOS PALSAR (2006 December–2010 December, 20 scenes) were used to cover the period until the beginning of the unrest. The changes of ground displacements within the unrest phase are monitored by processing independently 12 ENVISAT ASAR scenes (IS6) acquired between 2011 March and 2012 March in descending orbit (track 093), after the de-orbiting of the satellite. As a complementary source of information, RADARSAT-2 C-band acquisitions for the period of 2012 June acquired in descending Fine (F23) mode were used to provide further insights on the evolution of the volcano deformation after the loss of ENVISAT in 2012 April. SAR data processing was performed using the GAMMA processing software.

Since no significant changes in the state of the volcano were expected for the quiescent period (1992–2010), the estimation of the average displacement rates by interferometric stacking (IS) along with a pixel-based least-squares solution for the phase time-series were considered adequate (Figs 2 and 3). Starting from multireference spatially unwrapped differential interferograms, the single reference time-series were obtained through the Singular Value Decomposition. In this instance, ERS and ENVISAT data were jointly processed, yet avoiding multisensor combinations, whereas large dispersion of spatial baselines in the PALSAR interferometric stack dictated the exclusion of some scenes from the analysis. Processing and compensation strategy for dealing with various error sources followed Papageorgiou *et al.* (2012). Further analysis involving the calculation of the vertical and the E–W components of motion were performed by combining the estimated ERS-ENVISAT ascending and descending displacement rates.

For the inflationary phase (2011–2012), the Interferometric Point Target Analysis toolbox (Werner *et al.* 2003) was used, which is GAMMA's implementation of Persistent Scatterer Interferometric (PSI) technique, to derive the complete displacement history, including the non-linear motion component, on point-like targets. The limited number of available scenes during the unrest phase imposed the adaptation of a multireference PSI approach (Wegmüller *et al.* 2010), deviating from the commonly applied single master processing schemes. Similar approaches have been proposed for the study of complex motion fields (e.g. Berardino *et al.* 2002; Hooper *et al.* 2004; Lanari *et al.* 2004). Attention was given throughout the PSI processing as the entire volcanic complex was subjected to intense deformation. Specifically, an inherited difficulty was the separation between the various phase contributing terms, because

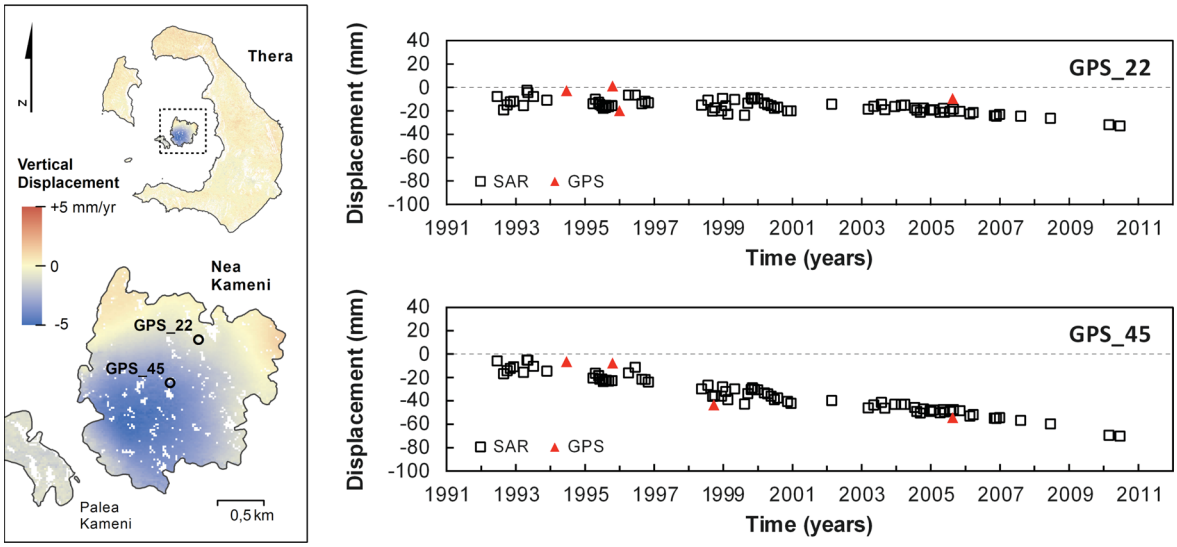

Figure 2. Vertical displacement time-series for the rest period (1992–2010) from combination of ascending and descending SAR acquisitions at GPS sites of Papageorgiou *et al.* (2010). The systematic linear motion trend at the area of the maximum observed subsidence on Nea Kammeni is evident.

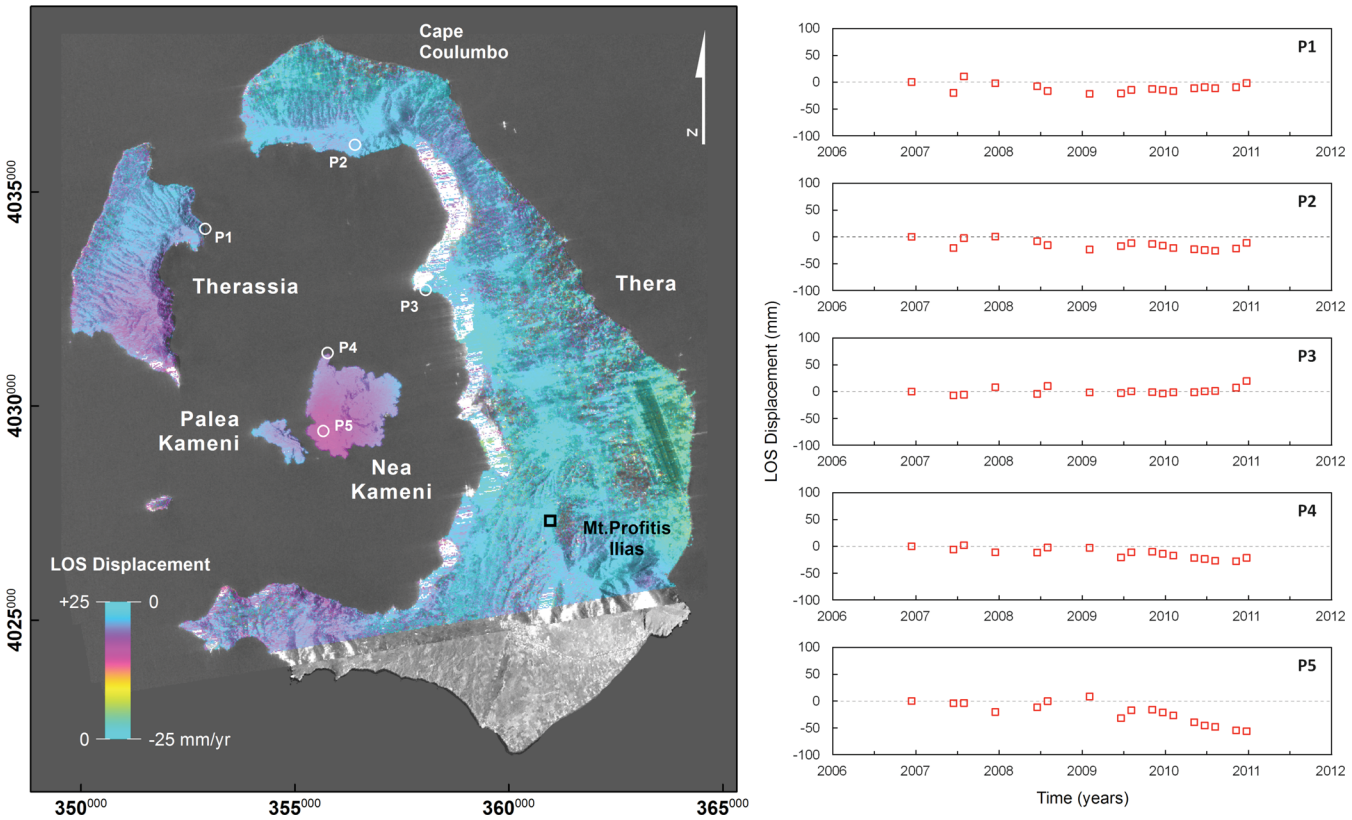

Figure 3. Average LOS displacement rates from PALSAR over the period 2006 December–2010 December. Temporal changes of ground displacements are shown by the deformation histories of selected locations. The location of the reference point is shown (square).

misallocation of the observed phase differences could directly lead to an overall underestimation of ground surface motion. Helpful to the analysis was that the perpendicular baselines were all less than 180 m relative to a reference track. This allowed the selection of pairs of consecutive acquisitions (short temporal intervals) instead of using an upper threshold on the maximum normal baseline value, avoiding significant phase changes between observations. Redundancy in the differential interferometric inputs reduces possible uncorrelated errors in the time-series, including residual topographic phase errors and phase noise. An iterative process was followed for a step-by-step improvement of height correction and deformation rates estimates following Wegmüller *et al.* (2010). The final PSI results include ground surface displacement rates, as well as the detailed deformation history of each point target, after compensating for orbital inaccuracies and atmospheric phase screen (Fig. 4).

Because SAR phase measurements are relative to a local reference point, to which zero deformation is assigned, a GPS site

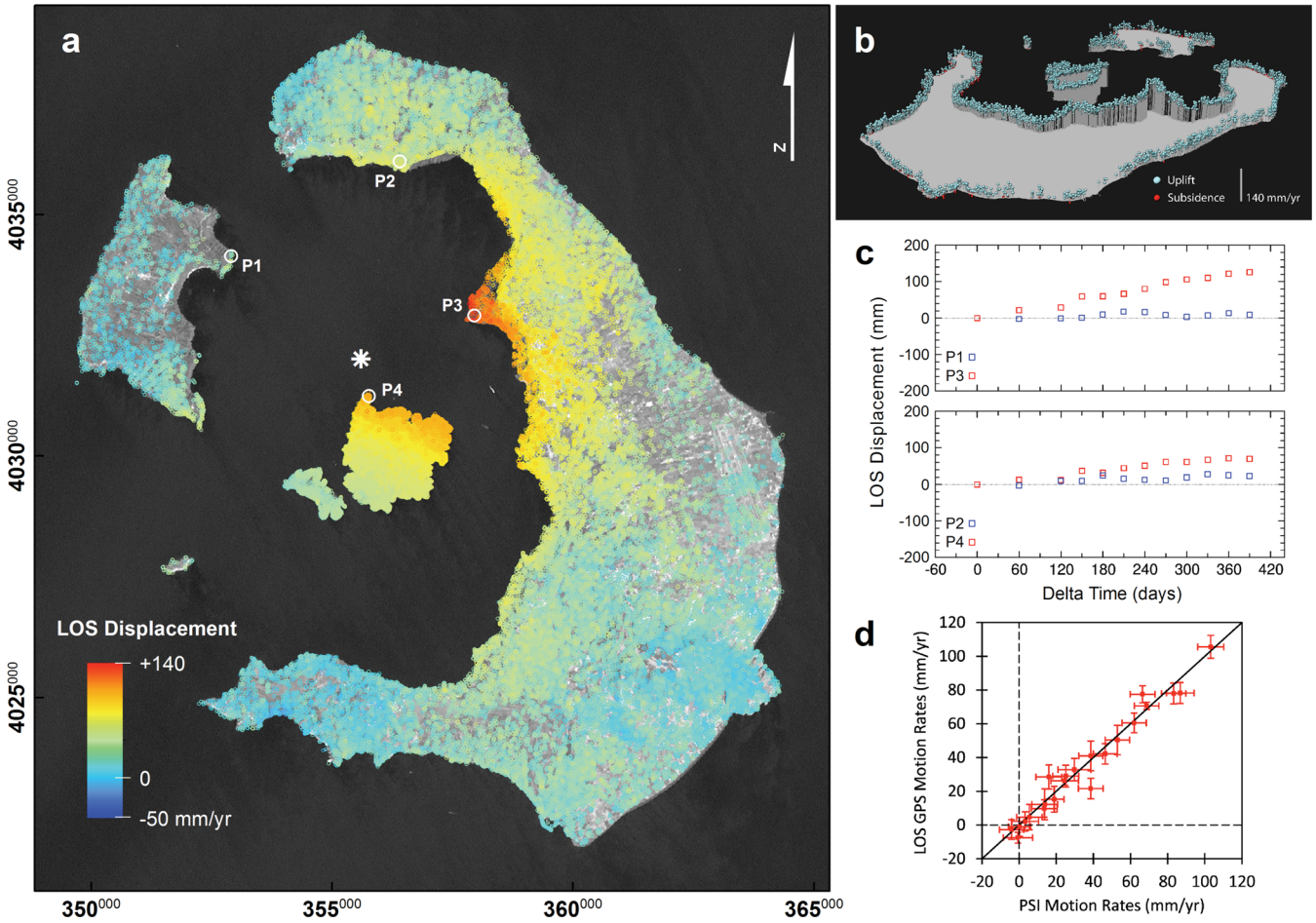

Figure 4. (a) PSI LOS displacement rates from ENVISAT ASAR data (2011 March–2012 March) showing the radial inflation pattern caused by the volcanic unrest, (b) perspective 3-D view of the point targets along the coastline of Santorini, (c) deformation histories of selected point targets and (d) correlation between GPS motion rates projected into the LOS geometry and PSI results after correction of reference frame, with error bars representing the 1-sigma confidence region.

(THR8) located at the southeastern part of Thera (Fig. 1), where the pre-volcanic basement outcrops, was selected to serve further exploitation of both data sets. However, an adjustment for the differences in the reference frames between these data sets had to be considered. Thus, the velocity of the selected GPS site was added to the SAR data set to compensate for the motion of the SAR reference point and to obtain the deformation relative to the GPS reference frame.

3 SOURCE MODELLING

The method implemented is a two-step inversion in which a global search is firstly performed in the parameters' space with the Neighbourhood Algorithm (NA), followed by a Bayesian (NAB) inference on the generated ensemble (Sambridge 1999a,b). This method has been largely tested in other volcanic regions (Trasatti *et al.* 2008). The volcanic sources adopted in this study are the isotropic point-source (Mogi 1958), hereafter called Mogi, and a finite volume 3-D spheroid arbitrary oriented in space (Yang *et al.* 1988), hereafter Yang. Despite the limits of a simplified spherical point-source, the Mogi source is still largely implemented in volcanic studies as it provides rapid and first-order estimates. A more accurate model is then preferred (Yang model), with additional degrees of freedom such as the spheroid axes and orientation.

4 REST PERIOD (1992–2010)

Volcano breathing was preceded by a period of rather negligible deformation. A noteworthy deformation feature observed during the 18 yr of observations is the concentric deflation pattern localized at the southern part of Nea Kameni, indicating prevalent subsidence of 5.2 ± 0.6 mm yr^{-1} (Fig. 1). The rest of the complex indicates rather low-displacement rates that do not exceed on average 1 mm yr^{-1}. The temporal variations of ground displacements determined through time-series analysis at the area of maximum subsidence are shown in Fig. 2.

To estimate the position and the annual rate of the volume change of a Mogi deflating pressure source, we subsampled the SAR data every 60 m. Results from the NAB inversion showed a shallow deflating isotropic source located at 800 ± 200 m b.s.l., undergoing a volume change rate of $-14 \pm 3 \times 10^3$ m^3 yr^{-1}. The source is located below the SW side of Nea Kameni, in accordance to the area of the maximum absolute velocity value (Fig. 1). From the combined ascending and descending SAR orbits in the east–west and vertical component, the source appears to be located along the east–west zero line and below the maximum vertical deformation (Fig. S1).

Similar deformation pattern is shown by ALOS PALSAR measurements (Fig. 3), yet slightly higher subsidence (up to 6.3 ± 1.8 mm yr^{-1}) compared to the ERS-ENVISAT rates were

calculated for the period until the beginning of 2010. Thereafter, an increased subsidence is observed in the deformation time-series, reaching about 3 cm over Nea Kameni. This signal gradually becomes less evident away from the northern part of the caldera, while is more apparent in the area of the modelled Mogi source. Finally, at the end of the observation time a reversal of motion was followed by a couple of centimetres of uplift, signifying the beginning of the inflation episode.

5 UNREST PHASE (2011–2012)

A pronounced change of the deformation pattern was observed during the period 2011–2012, related to relevant changes in the state of the volcano (Fig. 4). A characteristic radial inflation pattern is observed decreasing towards the external part of the caldera, underlining the volcanic nature of the deformation signal. According to SAR observations within the general uplift trend since the beginning of 2011, a cycling sequence of uplift and subsidence (Fig. 4c), typical of volcanic activity, is observed with apparent peaks during mid- and end-2011 (Fig. 5). Cumulative uplift on Nea Kameni reached almost 9 cm at the end of the observation period, while the maximum deformation of 14 cm was observed at Cape Skaros NNW of Fira. The above results are consistent with those obtained by Papageorgiou *et al.* (2012) over Nea Kameni until 2011 December.

A point targets density of approximately 1050 points km^{-2} was obtained, quite high value with respect to the urban signatures in Santorini, clearly attributed to the exposure of volcanic rocks due to the absence of vegetation, especially at Palea and Nea Kameni islands. Spatial continuity of PSI results allowed the detailed investigation of the volcanic induced deformation field. As an effect of the high-incidence angles (∼41°) of ASAR acquisitions (IS6), a significant portion of the horizontal motion detected by GPS (∼63 per cent of the E–W component) is included in the SAR line-of-sight (LOS) measurements.

The SAR data were subsampled every 200 m, obtaining a data set of about 2400 data points. We consider also the GPS measurements by Newman *et al.* (2012) to integrate the single orbit of the SAR observations. In particular, we consider the campaigns of 22 GPS stations for the time interval between the beginning of 2011 and 2011 August–2011 September. The compatibility between GPS and SAR results was checked by projecting GPS velocities into the SAR LOS geometry and comparing at these locations the PSI rates using linear regression. A correlation coefficient (R^2) of 0.96 was obtained, underlining the consistency between the independent results (Fig. 4d). From the signal variations of both data sets, the displacement trend may be considered with good approximation as linear with time. In the following we consider the whole unrest period, from the beginning of 2011 until the last available data of 2012 March and both GPS and SAR were scaled to cover the selected

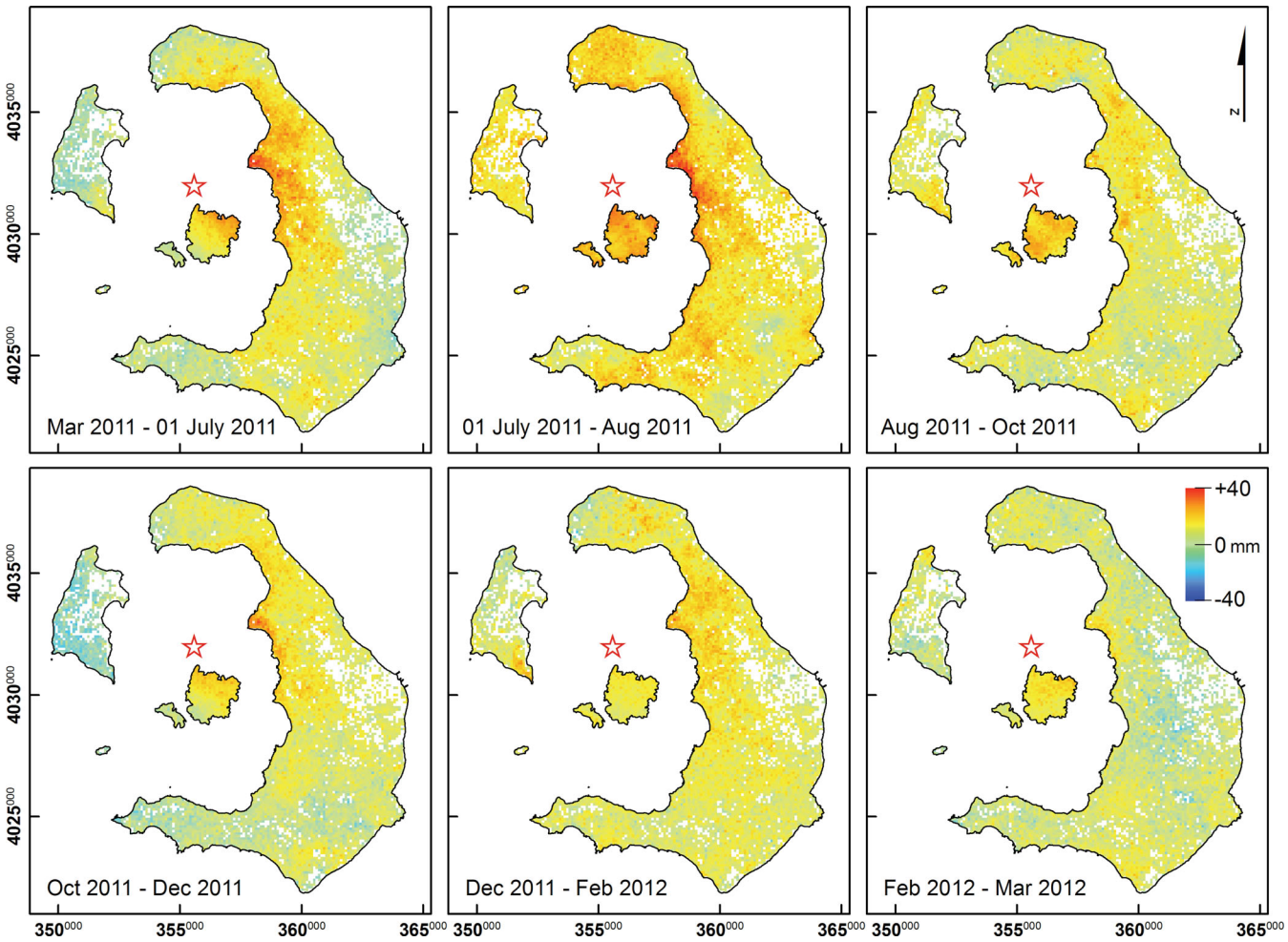

Figure 5. Spatio-temporal evolution of ground displacements during the unrest phase based on PSI time-series. The star marks the inferred horizontal position of the modelled deformation source.

Table 1. Parameters retrieved by the NAB inversion for the period 2011 January–2012 March, for the models considered.

Model	Total misfit[a]	GPS[b] weight	Easting[c] (km)	Northing[c] (km)	Depth (km)	ΔV (10^6 m^3)	Strike[d] (°)	Dip (°)	a[e] (m)	a/b[f]
Mogi[g]	6.8	50 per cent	355.6 ± 0.4	4032.3 ± 0.4	3.8 ± 0.4	11.4 ± 1	–	–	–	–
Yang[g]	4.8	50 per cent	355.6 ± 0.4	4032.0 ± 0.4	3.5 ± 0.5	7.5 ± 1	90 ± 10	60 ± 5	400 ± 50	4.6 ± 0.5
Mogi	4.0	0 per cent	355.6 ± 0.5	4032.7 ± 0.4	4.3 ± 0.5	11.7 ± 1	–	–	–	–
Mogi	8.4	100 per cent	355.6 ± 0.4	4032.2 ± 0.4	4.0 ± 0.4	12.8 ± 1	–	–	–	–
Yang	3.9	0 per cent	355.6 ± 0.7	4033.3 ± 0.7	4.2 ± 0.7	8 ± 1	100 ± 10	und.	und.	und.
Yang	4.9	100 per cent	355.6 ± 0.4	4033.3 ± 0.4	3.8 ± 0.5	9 ± 1	90 ± 10	52 ± 5	und.	3.9 ± 0.5

[a]The misfit function is computed by summing the single GPS and SAR reduced χ^2 scaled for the relative weight associated.
[b]Percentage weight associated to the GPS data set. The SAR percentage weight is complementary to the GPS weight.
[c]Source position in UTM Zone 35 North projection (datum WGS'84).
[d]Strike positive from north clockwise.
[e]Semi-major axes of the spheroid.
[f]Spheroid axes ratio (b is the semi-minor axis).
[g]Models shown in Fig. 6.

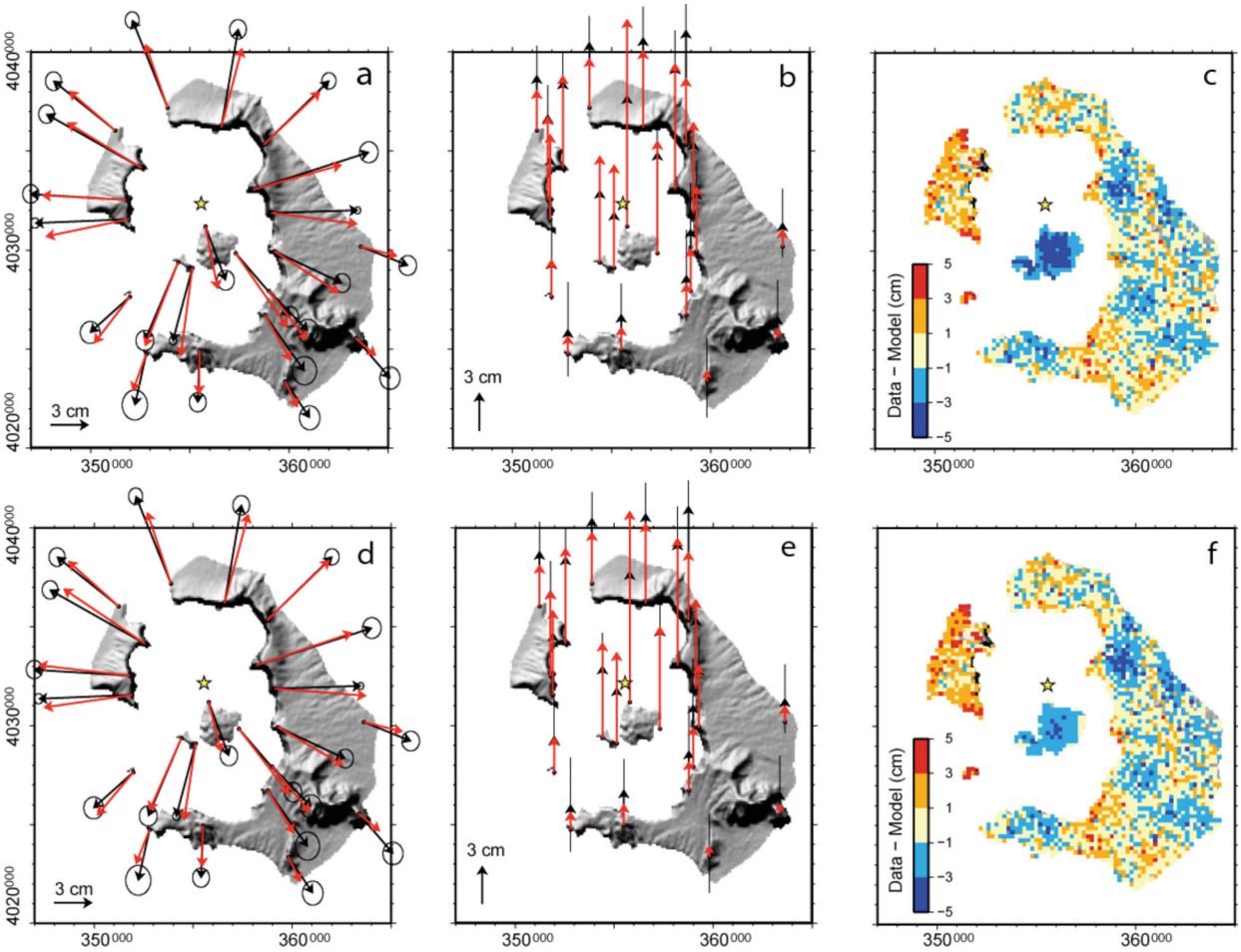

Figure 6. Results for the spherical source (Mogi; top) and the 3-D spheroidal source (Yang; bottom) for the period 2011 January–2012 March. (a–d) GPS horizontal data (black) compared to mean model (red). (b–e) GPS vertical data (black) compared to the mean model (red). (c–f) Residuals between PSI data and model. The yellow points are below data uncertainty. The yellow star indicates the source centre.

period of about 15 months. A series of inversions are computed to find a balance between the two data sets, as there is not a standard procedure to weight different data sets. After several attempts using different weights, a reasonable balance using a weight of 50 per cent for GPS and SAR for both Mogi and Yang sources were set.

The results of the inversions are reported in Table 1, including those obtained with single data sets, which are in agreement within error with those documented by Newman *et al.* (2012) and Parks *et al.* (2012) using GPS and SAR, respectively. In Fig. 6 the comparison between data and models for Mogi and Yang is shown. Both sources are located at about 1 km North of Nea Kameni at similar depths (3.8 km and 3.5 km, respectively). The volume variations of 11.4 × 10^6 m^3 for Mogi and 7.5 × 10^6 m^3 for Yang correspond to an annual rate of 9.2 × 10^6 m^3 yr^{-1} and 6.1 × 10^6 m^3 yr^{-1}, respectively. The additional Yang parameters describe a pressurized spheroid oriented east–west and dipping eastward of 60°. The spheroid parameters describing its shape, that is, the semi-axis a and the axes ratio a/b, are not well determined [see Fig. 7 for the

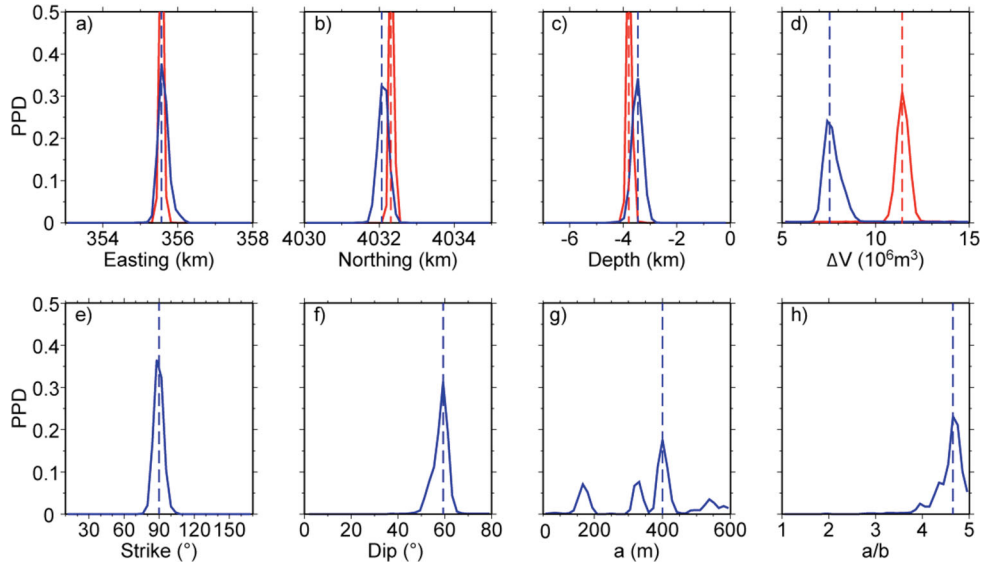

Figure 7. Posterior Probability Density (PPD) functions for the Mogi (red) and Yang (blue) parameters. The *strike* is computed from north clockwise, while *a* is the semi-major axis and *a/b* is the axes ratio. The vertical dashed lines represent the mean parameters retrieved by the Bayesian inference (NAB).

Posterior Probability Density (PPD) functions]. The use of the combined data sets improves the parameters' constraint. If we compare data fitting of the two different sources, the SAR-modelled data seems very similar (Fig. S2), while greater differences may be observed for the GPS data. The residuals between observed and computed SAR data (Figs 6c and f) show a comparable pattern with the exception of the central islands of Nea and Palea Kameni where both models overestimate the data. The same happens with the vertical GPS, overestimated in the central part of the caldera. The Yang source improves GPS fitting by enhancing the horizontal deformation and lowering the vertical GPS in Palea and Nea Kameni. This is confirmed by the retrieved misfits: the GPS misfit halves from 8.7 (Mogi) to 4.8 (Yang), while the SAR misfit is almost unchanged (from 4.9 to 4.7). This is due to the 3-D mapping of the GPS data that constrains the non-axi-symmetrical surface pattern of the spheroid, if compared to the single orbit of SAR.

A significant decrease of the ground deformation in the first quarter of 2012 is evident for the largest part of the volcanic complex, with the only area still exhibiting uplift being in the vicinity of the deformation source, however with decreased displacement rates. The above-mentioned trend is confirmed by the reduction of the number and the magnitude of the earthquakes occurring within the caldera, as well as with RADARSAT-2 interferometric results that show negligible deformation at the order of a few millimetres during 2012 June (Fig. 8).

6 CONCLUSIONS AND DISCUSSION

SAR results covering the period 1992–2010 mainly represent subsidence over Nea Kameni with rates of about 5–6 mm yr^{-1}. These findings are in agreement with GPS data (Papageorgiou *et al.* 2010). Inversion of the detected movements suggests a deflation source best constrained in the southern part of Nea Kammeni at 800 ± 200 m depth. In accordance with the absence of earthquakes within the intracaldera area, the dormant behaviour of the volcano is plausibly verified. From the geological point of view, the small size and shallow deformation source could be possibly associated to hydrothermal activity (e.g. low temperature venting), rather than to a deflating magma chamber.

Detailed SAR deformation histories for 1992–2010 (Fig. 2) imply that there was no significant magma intrusion episode at least for this time span. However, previous analysis of radial geodetic data from repeated electronic distance measurements have shown increased length of certain baselines (up to 10 cm) between 1994 and 2000, interpreted as small-scale aseismic inflation of the NW part of the caldera (Stiros *et al.* 2010). In fact, the comparable LOS motion rates presented herein between Nea Kameni and Therassia along the ascending and descending SAR orbits (7.1 mm yr^{-1} and 6.6 mm yr^{-1}, respectively, relative to Nea Kameni) indicate mainly vertical component, with negligible movements in the E–W direction. Thus, there should be significant N–S motion to justify such local baseline length increase, which cannot be detected by InSAR due to the lack of sensitivity along this direction. The presence of N–S motion, of lower magnitudes however, for almost the same period (1994–2005) is actually confirmed by measurements from a local GPS campaign network ($dN = 4.1$ mm yr^{-1}, $dE = -0.3$ mm yr^{-1}, $dU = 6.6$ mm yr^{-1}, relative to Nea Kameni; Papageorgiou *et al.* 2010); yet, neither signal was associated with some form of magmatic processes (emplacement). Nonetheless, the temporal sampling of campaign GPS observations is insufficient to provide detailed information. Parks *et al.* (2012) based on horizontal surface displacements from triangulation and GPS data showed no evidence for significant inflation of Santorini between 1955 and 2011, whereas if any deformation signal was subsequently reversed it cannot be verified.

The mean SAR velocities observed between 2011 March and 2012 March showed a radial uplift of the entire volcanic complex, reaching a maximum value of 14 cm. However, due to the submerged parts of the caldera, the maximum deformation is very likely underestimated, because the magmatic source (Mogi and Yang) was modelled offshore in the northern part of the caldera. The obtained results from the joint inversion modelling of space geodetic measurements confine a deformation source at the depth of 3.5–3.8 km. This confirms previous geological observations placing the post-Minoan magmatic activity at depths of 2–4 km (Barton & Huijsmans 1986; Francalanci *et al.* 1995).

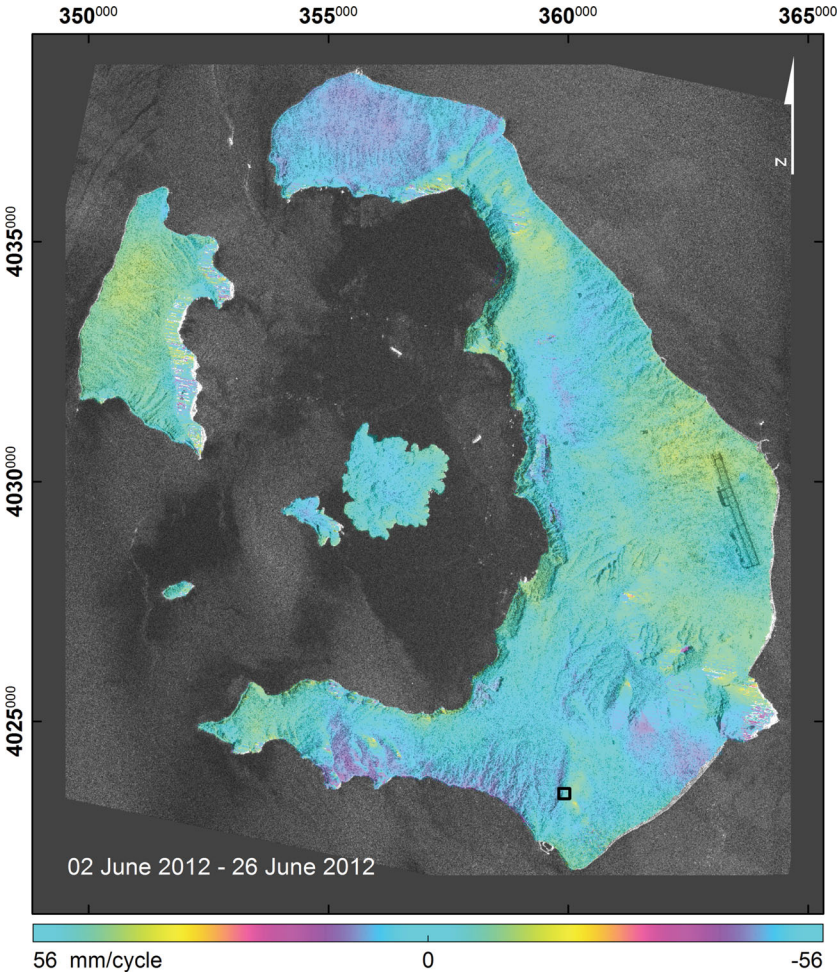

Figure 8. Unwrapped RADARSAT-2 differential interferogram for 2012 June (2012 June 2–2012 June 26, 24 days), with perpendicular baseline (Bp) of −184 m, showing reduced ground surface displacements of few millimetres where significant uplift was observed during the unrest episode. The location of the reference point is shown (square).

The recent volcanic activity was preceded, based on SAR measurements, by rapid subsidence adjacent to the deformation source. This motion occurred between 2010 February and 2010 May, and reached 1–3 cm in the following months; still was not accompanied by a corresponding change in seismicity. A subsequent reversal of motion since 2010 August marks the onset of the inflation phase. Indeed, changes in the pattern of degassing on Nea Kameni suggest increase of soil CO_2 emissions from 2010 September (Mather *et al.* 2012). The lack of continuous GPS recording stations in the vicinity of the deformation source suggests the capture of the inflation signal when the deformation field was expanded enough to affect the local monitoring network. The above facts underline the early warning capabilities and the importance for volcanic hazard monitoring in general, of spatially continuous observation systems such as space-borne SARs.

The short-period subsidence observed before the uplift could be seen as a preparatory phase of the following unrest providing interesting insights into the mechanism of the volcano deformation. Extraction of magma from deep reservoirs can result in compaction of the crustal column beneath the volcano (Druitt *et al.* 2012). Analogous condition is also indicated for the Minoan eruption. Druitt *et al.* (2012) describe that if the foundering in the Minoan reservoir had taken place rapidly enough, precursory uplift might have been greatly reduced. Substantial subsidence rates beneath growing magma reservoirs are compatible with theoretical models (Cruden 1998; Bachmann & Bergantz 2004).

Mogi and Yang magmatic sources were calculated using GPS and SAR separately and joined (Table 1). In all the optimizations the parameters and error (half width of the PPD function) were constrained. The results presented in Table 1 are comparable with those of Parks *et al.* (2012) and Newman *et al.* (2012) as is shown in the third and fourth line of Table 1, respectively. Newman *et al.* (2012) use GPS data and an isotropic (Mogi style but finite volume) source, obtaining an annual rate of 10.6×10^6 m^3 yr^{-1}, similar to our $10.4 \pm 1 \times 10^6$ m^3 yr^{-1}. Also the depths are equal, 4 km in both cases. Parks *et al.* (2012) invert a Mogi source with partially independent SAR data set at depth of 4.4 km, although in the same conditions we obtain a depth of 4.3 ± 0.5 km. It is evident that SAR data alone constrain a deeper source with respect to GPS data. Furthermore, their estimate for the total volume variation (2011 January–2010 April) of $15 + 7–3 \times 10^6$ m^3 yr^{-1} is compatible within uncertainties with our finding of $12 \pm 1 \times 10^6$ m^3 yr^{-1}. It should be noted that the horizontal position of the source centre is very well constrained as the difference is lower than 200 m and the associated error is 400 m.

The combined use of SAR and GPS for both models leads to slightly shallower sources and slightly lower volume variations than single data sets, but compatible within the associated errors,

evidencing a consistency between the displacements detected by both techniques. Using both data sets, we estimated volume variations of 11.4×10^6 m^3 and 7.5×10^6 m^3 for the Mogi and Yang sources, respectively, values which are outside the associated error (1×10^6 m^3). A reliable point-source approximation is however expected as we retrieve a semi-major axis $a = 400$ m, which is much lower of depth $d = 3500$ m, and it is confirmed by the bad constraining of a itself (Fig. 7). The discrepancy between the two-source volume changes may be attributed to the lower internal pressure required by non-isotropic source models such as spheroids and sills if compared to Mogi, to obtain the same surface deformation (Davis 1986). The nature of the pressurized source causing the observed deformation cannot be though defined, because integration with additional geophysical data (mainly gravity and chemical) is required to discern between its hydrothermal and magmatic origin.

The obtained spheroid, oriented along the east–west direction, is partly aligned to the Kameni volcano-tectonic system that controlled a major portion of the historic volcanic activity of Santorini (Druitt *et al.* 1989; Fytikas *et al.* 1990; Pyle & Elliott 2006) and was identified by soil gas surveys (Barberi & Carapezza 1994) among the most probable sites for future volcanic activity. There is a partial compatibility with the seismicity trend as well (Fig. 1), showing a strike of N50°–N70°. Although a correlation between the deformation source and the observed seismicity is not straightforward, the hypothesis of the impact of the local fault systems on volcanic processes cannot be ruled out. The presence of conductive zones collocated with existent fault zones were actually revealed by magnetotelluric surveys (Papageorgiou *et al.* 2010).

The rapid magma supply from depth and the significant fraction of volume intruded since early 2011 as compared to previous eruptions denote a possibility of an eruption in the future (Hooper 2012). Given the nearly present state of the volcano, as depicted by the evolution in time of both ground displacements during this inflationary episode (2011–2012) and RADARSAT-2 data during its termination, the recession of the phenomenon is apparently proved. However, further monitoring will show whether this episodic inflation is part of a longer term cyclic sequence of inflation and deflation episodes that might lead to an eruption or not, ensuring the preparedness in terms of hazard and risk assessment.

ACKNOWLEDGMENTS

Part of the work was carried within the frame of ESA's Terrafirma project. The authors would like to acknowledge ESA for ERS & ENVISAT and JAXA for ALOS data provision. GPS data were kindly provided by Andy Newman. RADARSAT-2 scenes were provided by MDA as part of ESA collaboration agreement. We are grateful to H. Laur for his support, M. Bonafede and A. Hooper for useful comments and suggestions and D. Pyle and C. Werner for their reviews that helped us improve the manuscript.

REFERENCES

Aristotle University of Thessaloniki (AUTH), Department of Geophysics, Earthquake Catalogue. Available at http://geophysics.geo.auth.gr/ss10.1093/gji/ggs135.html.

Bachmann, O. & Bergantz, G.W., 2004. On the origin of crystal-poor rhyolites: extracted from batholithic crystal mushes, *J. Petrol.,* **45,** 1565–1582.

Barberi, F. & Carapezza, M.L., 1994. Helium and CO_2 soil gas emission from Santorini (Greece), *Bull. Volcanol.,* **56,** 335–342.

Barton, M. & Huijsmans, J., 1986. Post-caldera dacities from the Santorini complex, Aegean Sea, Greece: an example of the eruption of lavas of near constant composition over a 2200 year period, *Mineral. Petrol.,* **94,** 472–495.

Berardino, P., Fornaro, G., Lanari, R. & Sansosti, E., 2002. A new algorithm for surface deformation monitoring based on small baseline differential SAR interferograms, *IEEE Trans. Geosci. Remote Sens.,* **40**(11), 2375–2383.

Bohnhoff, M., Rische, M., Meier, T., Becker, D., Stavrakakis, G. & Harjes, H.-P., 2006. Microseismic activity in the Hellenic Volcanic Arc, Greece, with emphasis on the seismotectonic setting of the Santorini–Amorgos zone, *Tectonophysics,* **423,** 17–33.

Chiodini, G. *et al.*, 1996. Fluid geochemistry for the surveillance of Thera Island, Final report 6/1996, Santorini volcano laboratory program, Project: Environnent EV5V-CT93-0285, 68 p.

Chiodini, G., Cioni, R., Guidi, M., Raco, B. & Marini, L., 1998. Soil CO_2 flux measurements in volcanic and geothermal areas, *Appl. Geochem.,* **13,** 543–552.

Cruden, A.R., 1998. On the emplacement of tabular granites, *J. Geol. Soc. Lond.,* **155,** 853–862.

Davis, P., 1986. Surface deformation due to inflation of an arbitrarily oriented triaxial ellipsoidal cavity in an elastic half-space, with reference to Kilauea volcano, Hawaii, *J. geophys. Res.,* **91,** 7429–7438.

Delibasis, N., Chailas, S., Lagios, E. & Drakopoulos, J., 1989. Surveillance of Thera volcano, Greece: microseismicity monitoring, in *Proceedings of the 3rd International Congress "Thera and the Aegean World",* Vol. 2, September 3–9, Santorini, Greece, pp. 199–206.

Dimitriadis, I., Karagianni, E., Panagiotopoulos, D., Papazachos, C., Hatzidimitriou, P., Bohnhoff, M., Rische, M. & Meier, T., 2009. Seismicity and active tectonics at Coloumbo Reef (Aegean Sea, Greece): monitoring an active volcano at Santorini Volcanic Center using a temporary seismic network, *Tectonophysics,* **465,** 136–149.

Dominey-Howes, D., Papadopoulos, G.A. & Dawson, A.G., 2000. Geological and historical investigation of the 1650 Mt Coloumbo (Thera island) eruption and tsunami, Aegean Sea, Greece, *Nat. Hazards,* **21,** 83–96.

Druitt, T.H., Mellors, R.A., Pyle, D.M. & Sparks, R.S.J., 1989. Explosive volcanism on Santorini, Greece, *Geol. Mag.,* **126,** 95–126.

Druitt, T.H., Edwards, L., Mellors, R.A., Pyle, D.M., Sparks, R.S.J., Lanphere, M., Davies, M. & Barreirio, B., 1999. Santorini volcano, *Geol. Soc. London Mem.,* **19,** 165.

Druitt, T.H., Costa, F., Deloule, E., Dungan, M. & Scaillet, B., 2012. Decadal to monthly timescales of magma transfer and reservoir growth at a caldera volcano, *Nature,* **482,** 77–80.

Dzurisin, D., 2003. A comprehensive approach to monitoring volcano deformation as a window on the eruption cycle, *Rev. Geophys.,* **41**(1), 1001–1001.

Fouqué, F., 1879. *Santorin et ses eruptions,* Masson et Cie., Paris, 440 pp.

Francalanci, L., Vougioukalakis, G., Pinarelli, L., Petrone, C. & Eleftheriadis, G., 1995. Interaction between mafic and acid magmas: the case study of the post Minoan activity of the Santorini volcanic field, Greece, *Plinius,* **14,** 166–167.

Friedrich, W.L., Kromer, B., Friedrich, M., Heinemeier, J., Pfeiffer, T. & Talamo, S., 2006. Santorini eruption radiocarbon dated to 1627–1600 B.C., *Science,* **312**(5773), 548.

Fytikas, M., Kolios, N. & Vougioukalakis, G., 1990. Post-Minoan volcanic activity of Santorini volcano. Volcanic hazard and risk, forecasting possibilities, in *Thera and the Aegean World III,* Vol. 2, pp. 183–198, eds. Hardy, D.A., Keller, J., Galanopoulos, V.P., Flemming, N.C. & Druitt, T.H., The Thera Foundation, London.

Georgalas, G., 1962. *Catalogue of the Active Volcanoes of the World, Including Solfatara Fields. Part 12, Greece,* International Association of Volcano, Rome, Italy, 40 pp.

Hooper, A., 2012. A volcano's sharp intake of breath, *Nature Geosci.,* **5,** 686–687.

Hooper, A., Zebker, H., Segall, P. & Kampes, B., 2004. A new method for measuring deformation on volcanoes and other natural terrains using InSAR persistent scatterers, *Geophys. Res. Lett.,* **31**(23), L23611.

Lanari, R., Mora, O., Manunta, M., Mallorqui, J.J., Berardino, P. & Sansosti, E., 2004. A small-baseline approach for investigating deformations

on full-resolution differential SAR interferograms, *IEEE Trans. Geosci. Remote Sens.,* **42**(7), 1377–1386.

Massonnet, D., Briole, P. & Arnaud, A., 1995. Deflation of Mount Etna monitored by spaceborne radar interferometry, *Nature,* **375,** 567–570.

Mather, T.A. *et al.*, 2012. Distinguishing sources of diffuse CO_2 emissions using ^{222}Rn-δ^{13}C systematics at Santorini Volcano, Greece, Abstract 1488500 presented at 2012 Fall Meeting, AGU, San Francisco, CA, December 3–7.

McCoy, F.W. & Dunn, S.E., 2002. Modelling the climatic effects of the LBA eruption of Thera: new calculations of Tephra volumes may suggest a significantly larger eruption than previously reported, in *Chapman Conference on Volcanism and the Earth's Atmosphere,* American Geographical Union, Thera, Greece, 21–22.

Mogi, K., 1958. Relations between the eruptions of various volcanoes and the deformations of the ground surfaces around them, *Bull. Earthq. Res. Inst. Univ. Tokyo,* **36,** 99–134.

National Observatory of Athens (NOA), Institute of Geodynamics, Hellenic Seismological Broadband Network (NOA_HL), Catalogue of revised locations. Available at http://bbnet.gein.noa.gr.

Newman, A.V. *et al.*, 2012. Recent geodetic unrest at Santorini Caldera, Greece, *Geophys. Res. Lett.,* **39,** L06309.

Nomikou, P., Carey, S., Papanikolaou, D., Croff Bell, K., Sakellariou, D., Alexandri, M. & Bejelou, K., 2012. Submarine volcanoes of Kolumbo volcanic zone NE of Santorini Caldera, Greece, *Glob. Planet. Change,* **90–91,** 135–151.

Papageorgiou, E., Tzanis, A., Sotiropoulos, P. & Lagios, E., 2010. DGPS and magnetotelluric constraints on the contemporary tectonics of the Santorini volcanic complex, Greece, *Bull. Geol. Soc. Greece,* **43**(1), 344–356.

Papageorgiou, E., Foumelis, M. & Parcharidis, I., 2012. Long- and short-term deformation monitoring of Santorini Volcano: unrest evidence by DInSAR analysis, *IEEE J-STARS,* doi:10.1109/JSTARS.2012.2198871.

Parks, M.M. *et al.*, 2012. Evolution of Santorini volcano dominated by episodic and rapid fluxes of melt from depth, *Nature Geosci.,* **5,** 749–754.

Perissoratis, C., 1995. *Surface Sediment Map of the Aegean Sea Floor, With Explanatory Text, Sheet Santorini (Thira), Scale 1:200,000,* Institute of Geological Mining and Expedition, Athens, Greece.

Pritchard, M.E. & Simons, M., 2002. A satellite geodetic survey of large-scale deformation of centres in the central Andes, *Nature,* **418,** 167–171.

Pyle, D.M. & Elliott, J., 2006. Quantitative morphology, recent evolution, and future activity of the Kameni Islands volcano, Santorini, Greece, *Geosphere,* **2**(5), 253–268.

Rosen, P., Hensley, S., Zebker, H.A., Webb, F.H. & Fielding, E.J., 1996. Surface deformation and coherence measurements of Kilauea Volcano, Hawaii, from SIR-C radar interferometry, *J. geophys. Res.,* **101**(E10), 23 109–23 125.

Sambridge, M., 1999a. Geophysical inversion with a Neighbourhood Algorithm - I. Searching a parameter space, *Geophys. J. Int.,* **138,** 479–494.

Sambridge, M., 1999b. Geophysical inversion with a Neighbourhood Algorithm - II. Appraising the ensemble, *Geophys. J. Int.,* **138,** 727–746.

Sigmundsson, F., Durand, P. & Massonnet, D., 1999. Opening of an eruptive fissure and seaward displacement at Piton de la Fournaise volcano measured by RADARSAT satellite radar interferometry, *Geophys. Res. Lett.,* **26,** 533–536.

Sigurdsson, H. *et al.*, 2006. Marine investigations of Greece's Santorini volcanic field, *EOS,* **87**(34), 337–348.

Stiros, S.C., Psimoulis, P., Vougioukalakis, G. & Fyticas, M., 2010. Geodetic evidence and modeling of slow, small-scale inflation episode in the Thera (Santorini) volcano caldera, Aegean Sea, *Tectonophysics,* **494,** 180–190.

Tizzani, P., Berardino, P., Casu, F., Euillades, P., Manzo, M., Ricciardi, G.P., Zeni, G. & Lanari, R., 2007. Surface deformation of Long Valley caldera and Mono Basin, California, investigated with the SBAS-InSAR approach, *Remote Sens. Environ.,* **108,** 277–289.

Trasatti, E. *et al.*, 2008. The 2004–2006 uplift episode at Campi Flegrei caldera (Italy): constraints from SBAS-DInSAR ENVISAT data and Bayesian source inference, *Geophys. Res. Lett,* **35,** doi:10.1029/2007GL033091.

Vougioukalakis, G. & Fytikas, M., 2005. Volcanic hazards in the Aegean area, relative risk evaluation, monitoring and present state of the active volcanic centers, in *The South Aegean Active Volcanic Arc – Present Knowledge and Future Perspectives,* Vol. 7, pp. 161–183, eds. Fytikas, M. & Vougioukalakis, G., Elsevier Series Developments in Volcanology.

Wegmüller, U., Walter, D., Spreckels, V. & Werner, C.L., 2010. Nonuniform ground motion monitoring with TerraSAR-X Persistent Scatterer Interferometry, *IEEE Trans. Geosci. Remote Sens.,* **48**(2), 895–904.

Werner, C., Wegmüller, U., Strozzi, T. & Wiesmann, A., 2003. Interferometric point target analysis for deformation mapping, in *Proceedings of. IGARSS,* Toulouse, France, 21–25 July, pp. 4362–4364.

Yang, X., Davis, P.M. & Dieterich, J.H., 1988. Deformation from inflation of a dipping finite prolate spheroid in an elastic halfspace as a model for volcanic stressing, *J. geophys. Res.,* **93,** 4249–4257.

SUPPORTING INFORMATION

Additional Supporting Information may be found in the online version of this article:

Figure S1. Results of the modelling of the 1992–2010 ERS-ENVISAT ascending and descending data. The two orbits are transformed into (a) east–west and (b) vertical data. Modelled (c) east–west and (d) vertical components are shown. The isotropic source (Mogi) is located at the east–west zero line and at the centre of the maximum vertical deformation (yellow star).

Figure S2. SAR-modelled data for (a) Mogi and (b) Yang models. The yellow star indicates the source centre (http://gji.oxfordjournals.org/lookup/supp1/doi:10.1093/gji/ggs135/-/DC1).

Please note: Oxford University Press are not responsible for the content or functionality of any supporting materials supplied by the authors. Any queries (other than missing material) should be directed to the corresponding author for the article.